Plasmonics (2022) 17:1751–1764
https://doi.org/10.1007/s11468-022-01662-3

Detection of Blood Plasma Concentration Theoretically Using SPR-Based Biosensor Employing Black Phosphor Layers and Different Metals

Abdulkarem H. M. Almawgani[1] · Malek G. Daher[2] · Sofyan A. Taya[2] · Melad M. Olaimat[3] · Adam R. H. Alhawari[1] · Ilhamic Colak[4]

Received: 30 March 2022 / Accepted: 27 May 2022 / Published online: 6 June 2022

Abstract
The main role of blood plasma is to transport proteins, hormones, and nutrients to certain parts of the body. All blood constituents are carried by blood plasma through the circulatory system. Cells get rid of waste products into the plasma. In this paper, we present a surface plasmon resonance (SPR) biosensor based on a black phosphor (BP) layer to improve the sensor performance. The black phosphor layer is employed as an interacting medium with the sensing medium for the improvement of the sensor sensitivity. The sensor is employed for the detection of blood plasma. Four metals are used: silver (Ag), gold (Au), copper (Cu), and aluminum (Al). We found that structures with the BP layer have better performance than those without a BP layer. Cu-structure has shown the highest sensitivity while the Ag-structure has shown the highest quality factor and detection accuracy and the lowest FWHM. As the concentration of the plasma increases, the sensitivity can be enhanced.

Keywords Surface plasmon resonance · Plasma concentration · Sensor · Black phosphor · Sensitivity

Introduction

Surface plasmon resonance (SPR) is a powerful optical technique that is utilized in enzyme and chemical detection, medical diagnostics, and the safety of food [1–4]. These SPR approaches have been widely utilized to detect a variety of physical and biological markers quickly and accurately. The attenuated total reflection (ATR) approach, in which transverse magnetic (TM) incident radiation stimulates a surface plasmon wave along with the dielectric-metal interface, can be employed in the majority of SPR-based sensors. In ATR configurations, a thin layer of metal is usually deposited on the base of a prism [5]. One of the most important aspects of creating SPR-based applications is the selection of metallic film. In the traditional SPR biosensors, the active metals that are usually utilized are silver (Ag), gold (Au), aluminum (Al), copper (Cu), indium (In), and sodium (Na) [6]. Indium is costly and sodium is a good reactive in nature. Copper, silver, and aluminum are oxidation-susceptible. Gold can resist corrosion and oxidation in a variety of environmental conditions and is the most useful metal in nature. In SPR-based sensors, gold shows high sensitivity, and in general, it has good chemical stability. Compared to most metals, gold is considered relatively expensive. Silver, on the other hand, has superior resolution but is more prone to oxidation than gold. The Au/Ag bimetallic combination has been proposed to take the advantage of both metals and has been widely used. Several research works have been published on this. It is observed that the bimetallic film can enhance the SPR resolution but the sensitivity does not show a substantial improvement [7, 8]. As a result of its direct and tunable bandgap, outstanding optical and electrical characteristics, and increased mobility of the carriers [9–12], black phosphorus (BP) has recently been recognized as a promising medium for SPR applications [13]. BP is a phosphorus allotrope made up of many layers with two-dimensional

✉ Sofyan A. Taya
staya@iugaza.edu.ps

1 Electrical Engineering Department, College of Engineering, Najran University, Najran, Kingdom of Saudi Arabia

2 Physics Department, Islamic University of Gaza, P.O. Box 108, Gaza, Palestine

3 Al Al-Bayt University, P.O. Box 130040, Mafraq 25113, Jordan

4 Department of Electrical and Electronics Engineering, Nisantasi University, Istanbul, Turkey

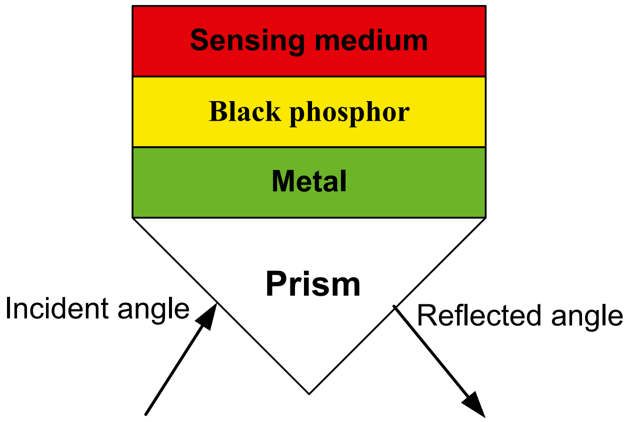

Fig. 1 An SPR structure based on a BP layer

Table 1 Refractive indices and extinction coefficients of all materials at a light wavelength of 632.8 nm

Material	Refractive index (n)	Extinction coefficient (k)	Reference
N-FK51A glass	1.4853	-	[29]
Au	0.1433	3.6080	[6]
Ag	0.051255	4.3165	[6]
Cu	0.10926	3.5802	[6]
Al	1.1528	6.6898	[6]
BP	3.5	0.01	[30]

structures that are held together by van der Waals forces. The BP also has appealing mechanical, chemical, and physical features, making it a good option for chemical applications with high-performance potential [14]. The in-plane anisotropy of phosphorene, which results from its sp^3 hybridized puckered lattice structure [15–18], is its most remarkable characteristic. The phosphorene's in-plane anisotropy can be used to create a tunable sensing device. The strongest plasmon excitation on the metal–BP interface is considered through a rotation angle of the integrated device around the z-axis in-plane, and as a result, the charge transfer between BP and the metal is changed, leading to modification in the minimum reflectivity.

BP is a two-dimensional stable material having tunable bandgap (0.3–2 eV), outstanding hole mobility (10,000 $cm^2 \cdot V^{-1} \cdot s^{-1}$), strong binding energy, attention-grabbing puckered surface morphology, hydrophilic nature, about 40 times higher molar response factor, and parts per billion sensing capability. It has shown great potential for biosensing, humidity, and gas sensing [19–23].

Despite several investigations into the nano- and optoelectronic applications of BP, including photonic applications based on its saturable absorption properties, little attention has been dedicated to its potential biomedical application [24]. This could be owing to black phosphorus's inability to maintain its stability when exposed to water or air. Several recent researches have shown that it is possible to synthesize new BP nanostructures that are stable in water

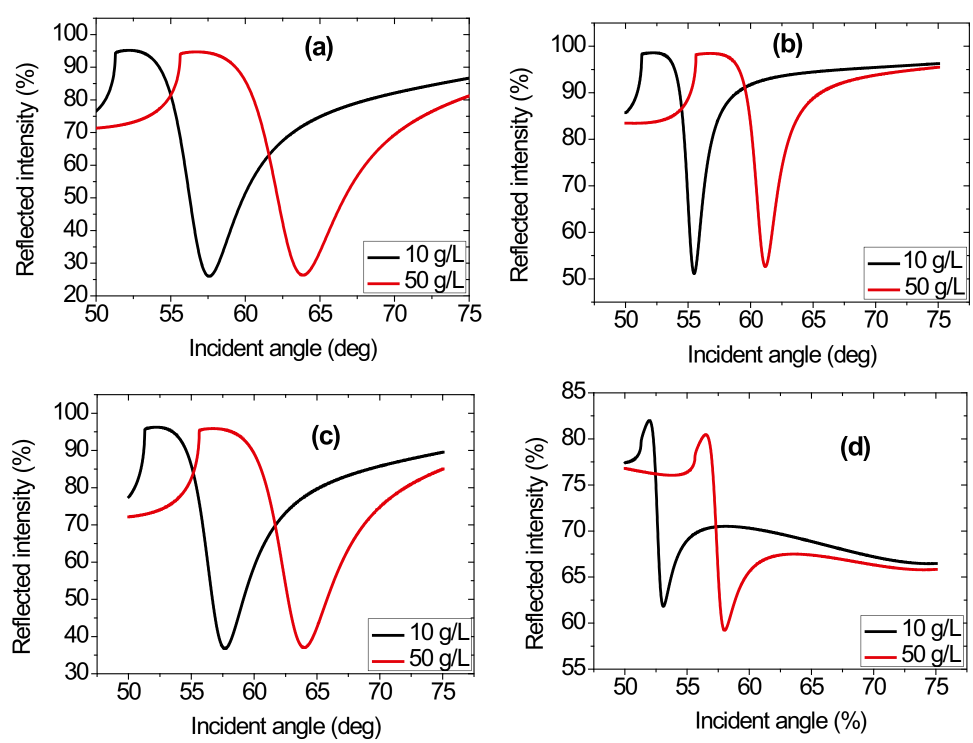

Fig. 2 Reflected intensity versus the angle of incidence without a BP layer. **a** With Au, **b** with Ag, **c** with Cu, and **d** with Al at λ = 632.8 nm and d_m = 35 nm

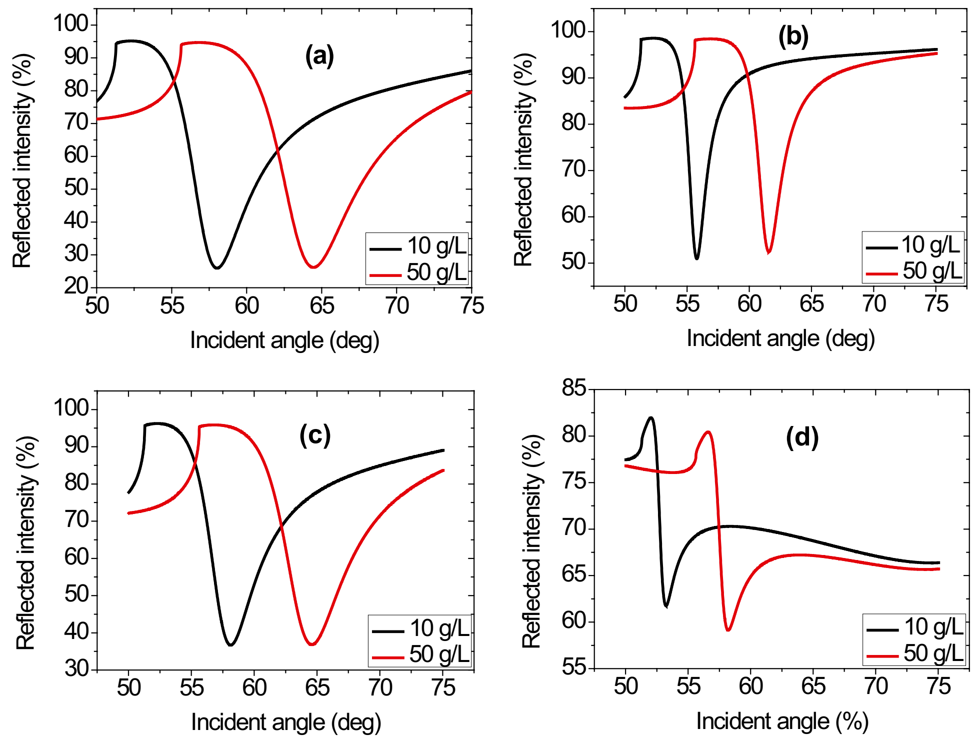

Fig. 3 Reflected intensity versus the angle of incidence with a BP layer. **a** With Au, **b** with Ag, **c** with Cu, and **d** with Al at λ = 632.8 nm and $d_m = 35$ nm

and air [25]. Phosphorus, which is used to synthesize BP, is a healthy, important element that acts as a bone ingredient, accounting for about 1% of total body weight. Phosphorus, being one of the key components of nucleic acids, is essential for human health, resulting in a biocompatible substance with broad biological application potential [26].

According to Srivastava et al., adding a layer of BP to the SPR sensors can enhance sensitivity [27]. Graphene, on the other hand, has recently been discovered to have extraordinary features such as high charge carrier mobility, which results in strong coupling at the metal-graphene interface [27]. When compared to a typical gold-based SPR biosensor, Wu et al. found that using graphene can enhance the sensitivity of such sensors [28].

The yellow liquid that makes up half of a person's blood is called plasma. Blood plasma is essential for combating infection, regulating blood pH, assisting blood clotting, and transporting and removing waste materials. The concentration of an agent in plasma generated from whole blood is referred to as plasma concentration. Major pharmacokinetics (drug movement through the body) and pharmacodynamics (biological response of the body to drugs) parameters are defined using plasma concentrations.

A four-layer SPR-based biosensor is proposed for the detection of blood plasma concentration. The sensor employs a layer of BP two-dimensional material. We will investigate the performance of different metals (Au, Ag, Cu, and Al). The novelty of the current work is proposing an SPR-based blood plasma concentration biosensor using BP two-dimensional material since it has recently been recognized as a promising material with outstanding properties.

Design and Model

Design Considerations

An SPR-based biosensor is assumed in this communication. The aim of the work is the detection of plasma concentration. The structure consists of four layers: N-FK51A glass prism, metal, BP, and sensing medium. It was shown in a

Table 2 Minimum reflectance, change of resonant angle, and sensitivity for different metals with/without BP layer at λ = 632.8 nm and $d_m = 35$ nm (The minimum reflectance is measured at a plasma concentration of 50 g/L)

Metal	With or without BP layer	Minimum reflectance (%)	Resonant angle shift (deg.)	Sensitivity (deg./RIU)
Au	Without BP layer	25.19	6.2	79.81
Ag		52.54	5.74	73.89
Cu		36.24	6.3	81.10
Al		58.34	4.93	63.46
Au	With BP layer	25.19	6.41	82.51
Ag		52.96	5.81	74.79
Cu		36.81	6.45	83.03
Al		58.34	5.1	65.65

Table 3 Sensitivity, FWHM, DA, and QF for different thicknesses of Au and different numbers of BP layers

Thickness of Au (nm)	Number of BP (M)	Resonant angle shift (deg.)	Sensitivity (deg./RIU)	FWHM (deg.)	DA (1/deg.)	QF (1/RIU)
35	1	6.41	82.51	5.1	0.196	16.17
40	1	6.58	84.70	4.4	0.227	19.25
45	1	6.68	85.99	3.56	0.280	24.15
50	1	6.71	86.38	3.33	0.300	25.93
35	3	6.75	86.89	6.4	0.156	13.57
40	3	6.99	89.98	5.07	0.197	17.74
45	3	7.01	90.24	4.25	0.235	21.23
50	3	7.13	91.78	3.57	0.280	25.70
35	6	7.36	94.74	7.7	0.129	12.30
40	6	7.67	98.73	6.71	0.149	14.71
45	6	7.85	101.05	5.1	0.196	19.81
50	6	8.01	103.11	4.15	0.240	24.84
35	9	8.22	105.81	10.2	0.098	10.37
40	9	8.7	111.99	8.32	0.120	13.46
45	9	9.13	117.53	6.99	0.143	16.81
50	9	9.45	121.65	6.12	0.163	19.87

previous work that N-FK51A has a low refractive index and corresponds to a larger sensitivity compared to SF-10 prism [8].

Figure 1 shows a diagram of the SPR structure. The working principle of the proposed biosensor is based on surface plasmon resonance conditions. Surface plasmons are quanta of charge density oscillations at the interface separating the metal and dielectric layers that are excited by incident transverse magnetic light with coupling through the prism [15]. Prism coupling is a preferred technique over other techniques for its straightforward geometry. The condition of resonance can be achieved via matching of wavevector of the surface plasmon wave with that of the incident light. Because of the adsorption of the analyte on the sensor surface, this matching condition is sensitive to changes in the refractive index of the probing media, which can be exploited for imaging and sensing applications [15]. Here, a low refractive index prism is chosen for enhanced light coupling [8].

The index of refraction of the N-FK51A glass prism (n_p) is given by the Sellmeier equation as [29]:

$$n_p = \sqrt{1 + \frac{a_1\lambda^2}{\lambda^2 - b_1} + \frac{a_2\lambda^2}{\lambda^2 - b_2} + \frac{a_3\lambda^2}{\lambda^2 - b_3}} \tag{1}$$

where the coefficients have the values $a_1 = 0.971247817$, $a_2 = 0.216901417$, $a_3 = 0.904651666$, $b_1 = 0.00472301995$, $b_2 = 0.0153575612$, and $b_3 = 168.68133$. λ is the wavelength of incident radiation in μm.

The metal refractive index is given by:

$$n_{metal} = 1 - \frac{\lambda_c\lambda^2}{\lambda_p{}^2\left(\lambda_c + i\lambda\right)} \tag{2}$$

where λ_c and λ_p are the collision and plasma wavelengths of the metal. Equation (2) is called Drude-Lorentz model.

The refractive indices used for all layers are presented in Table 1. They have been calculated at the He–Ne laser wavelength.

Mathematical Modeling

The refractive index, permittivity, and thickness of any layer of the stack of layers shown in Fig. 1 are given by n_j, ε_j, and d_j, respectively. The tangential field components at boundary number 1 ($z = 0$) are related to those at boundary number N ($z = z_{N-1}$) through the characteristic matrix W:

$$\begin{bmatrix} F_1 \\ G_1 \end{bmatrix} = W \begin{bmatrix} F_{N-1} \\ G_{N-1} \end{bmatrix} \tag{3}$$

where F_1 and F_{N-1} are the tangential electric field components at the first and Nth interfaces, respectively. G_1 and G_{N-1} are the same for the magnetic fields. The characteristic matrix (W_j) for any layer is defined as follows:

$$W_j = \begin{bmatrix} \cos(\alpha_j) & -\frac{i\sin(\alpha_j)}{Y_j} \\ -iY_j\sin(\alpha_j) & \cos(\alpha_j) \end{bmatrix} \tag{4}$$

α_j is the phase variation given by:

$$\alpha_j = \frac{2\pi}{\lambda} d_j\left(\varepsilon_j - (n_1\sin\theta_1)^2\right)^{0.5} \tag{5}$$

where θ_1 and n_1 are the incident angle and refractive index of the prism, respectively. For transverse magnetic (TM) waves, $Y_j = \left(\varepsilon_j - (n_1\sin\theta_1)^2\right)^{0.5}/\varepsilon_j$. The characteristic matrix P of the whole structure is written as follows:

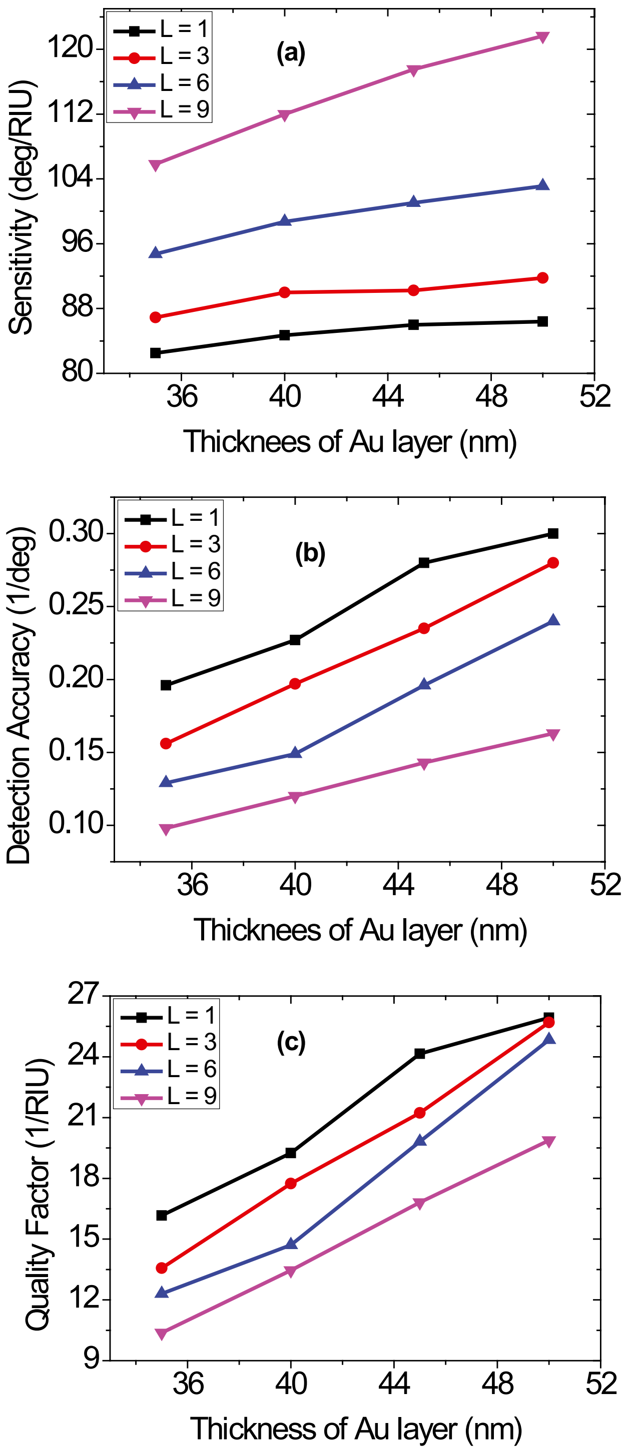

Fig. 4 The sensitivity (**a**), detection accuracy (**b**), and quality factor (**c**) versus the Au layer thickness for different numbers of BP layers at a light wavelength of 632.8 nm

$$P = W_{Ag} W_{BP} = \begin{bmatrix} P_{11} & P_{12} \\ P_{21} & P_{22} \end{bmatrix} \tag{6}$$

where W_{Ag} and W_{BP} are the transfer matrices of the metal and BP layers, respectively. For TM polarization, the reflection coefficient (r) is given by:

$$r = \frac{\left(P_{11} + P_{12}Y_N\right)Y_1 - \left(P_{21} + P_{22}Y_N\right)}{\left(P_{11} + P_{12}Y_N\right)Y_1 + \left(P_{21} + P_{22}Y_N\right)} \tag{7}$$

where P_{ij} are the total characteristic matrix elements. The reflection intensity (R) can be written in terms of the reflection coefficient as follows:

$$R = |r|^2 \tag{8}$$

Results and Discussion

An SPR-based biosensor with the structure prism, metal, BP, and sensing medium is assumed. Metal and BP layer thicknesses are d_m, and d_{BP} and the refractive indices are n_{m} and n_{BP}, respectively. At a radiation wavelength of 632.8 nm, n_m, n_{BP}, and n_p are calculated using the above equations.

We first investigate the sensor performance with and without a BP layer. In Figs. 2 and 3, the reflected intensity-incidence angle curves are plotted without (Fig. 2) and with (Fig. 3) BP layer for different metals of Au, Ag, Cu, and Al. The index of refraction of the sensing medium (plasma) is taken as 1.34401 and 1.42169 for concentrations of 10 g/L and 50 g/L, respectively. An N-FK51A glass prism is used as a coupler which has a low refractive index of 1.4853. It was shown that a low refractive index coupling prism gives a better performance in SPR structures than high index prisms [31]. The minimum reflectance, shift in resonance angle, and sensitivity are shown in Table 2. It is noted that the sensitivity has an enhancement when the BP layer is inserted between the metal and the sensing medium for all metals. The sensitivities of the biosensor with the structure of prism/metal/sensing medium are found as 79.81, 73.89, 81.10, and 63.46 deg./RIU for Au, Ag, Cu, and Al metals, respectively. The sensitivities of the structure prism/metal/BP/sensing medium are found as 82.51, 74.79, 83.03, and 65.65 deg./RIU for the metals Au, Ag, Cu, and Al, respectively. It is noted that the sensitivity for the Cu-metal structure is a little bit higher than other metal structures. The sensitivities for the Au- and Ag-metal structures are acceptable and they do not show a considerable deviation compared to that of the Cu-metal structure. The sensitivity associated with the Al-metal structure is the lowest. Moreover, it is clearly observed from the two Figs. (2 and 3) that the SPR curves for Cu, Au, and Ag are acceptable and in the normal shape but the curve is different for the Al-metal structure. Therefore, the

Table 4 Sensitivity, FWHM, DA, and QF for different thicknesses of Ag and different numbers of BP layers

Thickness of Ag (nm)	Number of BP (M)	Resonant angle shift (deg.)	Sensitivity (deg./RIU)	FWHM (deg.)	DA (1/deg.)	QF (1/RIU)
35	1	5.81	74.79	2.01	0.497	37.20
40	1	5.83	75.05	1.52	0.657	49.37
45	1	5.86	75.43	0.69	1.449	109.31
50	1	5.88	75.69	0.43	2.325	176.02
35	3	6.01	77.36	2.35	0.425	32.91
40	3	6.03	77.62	1.66	0.602	46.75
45	3	6.07	78.14	1.25	0.8	62.51
50	3	6.12	78.78	1.09	0.917	72.27
35	6	6.40	82.38	3.02	0.331	27.27
40	6	6.45	83.03	2.19	0.456	37.91
45	6	6.47	83.29	1.65	0.606	50.47
50	6	6.50	83.67	1.23	0.813	68.02
35	9	6.91	88.95	3.7	0.270	24.04
40	9	7.09	91.27	2.46	0.406	37.10
45	9	7.12	91.65	2.06	0.485	44.49
50	9	7.23	93.07	1.51	0.662	61.63

structures of Au, Ag, and Cu will be considered for further investigations.

The thickness of the metal layer and the number of BP layers must be optimized to provide the best biosensor performance. The suggested SPR biosensor's performance is assessed in terms of sensitivity (S), full width at half maximum (FWHM), detection accuracy (DA), and quality factor (QF). We will examine these parameters at different thicknesses of the metal layer and different numbers of the BP layers. The ratio of the shift in the resonance angle ($\Delta\theta_{res}$) to the change in the analyte's refractive index (Δn) defines the sensor sensitivity (S) [32],

$$S = \frac{\Delta\theta_{res}}{\Delta n} \tag{9}$$

The detection accuracy (DA) of a biosensor is given as the inversion of the FWHM which is given by:

$$DA = \frac{1}{\text{FWHM}} \tag{10}$$

The DA is an indicator of how sharp is the resonance dip.

The quality factor (QF) depends on the resonance dip shift and FWHM and is given by.

$$QF = \frac{S}{\text{FWHM}} = S \times DA \tag{11}$$

We start with the Au metal. Table 3 presents the sensing performance for some different combinations of the Au thickness and number of BP layers. The Au layer thickness ranges from 35 to 50 nm in steps of 5 nm and the number of BP takes the values 1, 3, 6, and 9. All the considered performance parameters (sensitivity, detection accuracy, and quality factor) can be enhanced with the increase of the Au layer thickness as shown in Fig. 4. Furthermore, it has been demonstrated that the number of BP layers has a considerable impact on the performance of the SPR biosensor. The sensitivity is shown to improve as the number of BP layers increases for a certain thickness of the Au layer. With an increase in the number of BP layers, both the detection accuracy and the quality factor are shown to decrease. With a 50-nm Au layer thickness and nine layers of BP, a maximum sensitivity of 121.65 deg./RIU can be attained. With an Au thickness of 50 nm and a monolayer of BP, the detection accuracy reaches a maximum of 0.300/deg. and the greatest quality factor of 25.93/RIU can be achieved. For a number of BP layers greater than 9, no resonant dip can be seen in the reflectance profile.

When the number of BP is kept fixed, the sharper dip with smaller FWHM is observed at higher thicknesses of the metal layer due to the minimum damping of surface plasmons [15].

Table 4 shows the same as Table 2 but for the Ag metal. For a constant number of BP layers, the sensitivity improves slightly as the thickness of the Ag layer increases, as illustrated in Fig. 5. In addition, as the thickness of the Ag layer increases, the detection accuracy and quality factor improve slightly. However, when a monolayer of BP is used, an ultra-enhancement of detection accuracy and quality factor can be observed for Ag-layer thicknesses greater than 40 nm. Furthermore, it is shown that the number of BP layers has a significant impact on the performance of the proposed SPR biosensor. Assuming that the thickness of the Au layer remains constant, the sensitivity improves as the number of BP layers increases.

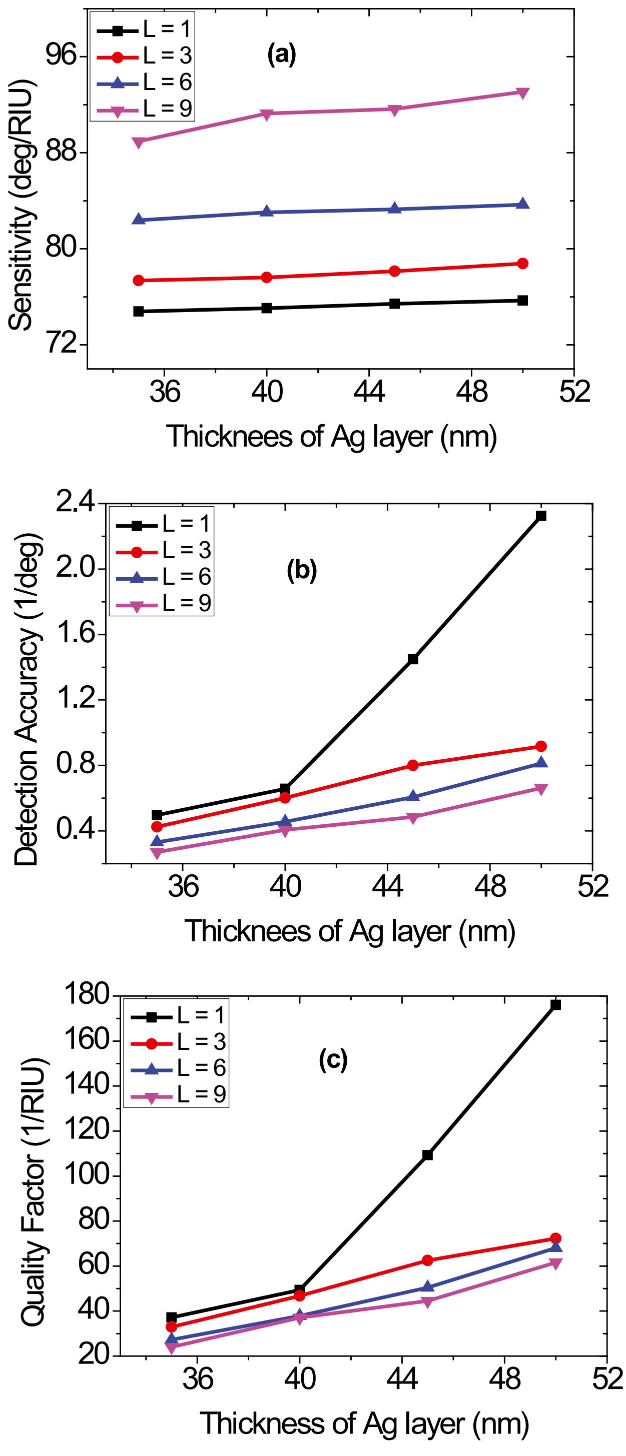

Fig. 5 The sensitivity (**a**), detection accuracy (**b**), and quality factor (**c**) versus the Ag layer thickness for different numbers of BP layers at a light wavelength of 632.8 nm

As an example, when a fixed 35-nm thickness of Ag is considered, the sensitivity is found as 74.79, 77.36, 82.38, and 88.95 deg./RIU for M = 1, 3, 6, and 9. However, as the number of BP layers grows, both the detection accuracy and quality factor are reduced. As an example, when a fixed 35-nm thickness of Ag is used, the detection accuracy and the quality factor are found as 0.497, 0.425, 0.331, and 0.270 and 37.20, 32.91, 27.27, and 24.04, respectively, for M = 1, 3, 6, and 9, respectively. We conclude that for the structure including the Ag metal layer, a thickness of 50 nm and nine layers of BP correspond to the highest sensitivity of 93.07 deg./RIU. With an Ag layer thickness of 50 nm and a monolayer of BP, the detection accuracy and quality factor reach a maximum of 2.325/deg. and 176.02 /RIU, respectively.

The sensing configurations for different Cu layer thicknesses and different numbers of the BP layer are presented in Table 5. As illustrated in Fig. 6, when the number of BP layers is fixed, the sensitivity, detection accuracy, and quality factor show improvements as the Cu layer thickness increases. Furthermore, it has been demonstrated that the number of BP layers can have a considerable effect on the SPR-based sensor performance. Assuming that the thickness of the Cu layer remains constant, the sensitivity enhances as the number of BP layers increases. For a number of BP layers of 1, 3, 6, and 9, the sensitivities are 85.09, 89.98, 99.51, and 113.41 deg./RIU when the thickness of Cu is fixed at 40 nm. In a similar manner to the previous investigations, the detection accuracy and quality factor show reduction as the number of BP layers grows. When the same thickness of Cu (40 nm) is utilized, the detection accuracy is found to be 0.251, 0.203, 0.162, and 0.125 for a number of BP layers of 1, 3, 6, and 9, respectively, while the quality factor is found as 21.43, 18.28, 16.12, and 14.26 for a number of BP layers of 1, 3, 6, and 9, respectively. It is concluded that, at a Cu thickness of 50 nm and nine layers of BP, the highest sensitivity of 123.97 deg./RIU is attained. With a thickness of Cu layer of 50 nm and a monolayer of BP, the detection accuracy and quality factor reach a maximum of 0.362 deg.$^{-1}$ and 31.43 RIU^{-1}, respectively.

From the above investigations, it is clear that Cu-structure has the highest sensitivity (123.97 deg./RIU) when the metal layer thickness is 50 nm and the number of BP layers is nine while the maximum sensitivities for Au- and Ag-structures are found 121 and 93 deg./RIU, respectively, at the same conditions. However, the Ag-structure has the highest detection accuracy (2.325/deg.) and the highest quality factor (176.02/RIU) at an Ag layer thickness of 50 nm and a monolayer of BP. Since sensitivity is the most important parameter of biosensors, we will consider in the next investigations a metal layer of 50 nm and a number of BP layers of nine.

The performance of the proposed biosensor is now evaluated for different concentrations of blood plasma. The optimum conditions will be considered here. Figure 7 shows the reflected intensity of the Au structure for different concentrations of blood plasma. The resonant angles corresponding to

Table 5 Sensitivity, FWHM, DA, and QF for different thicknesses of Cu and different numbers of BP layers

Thickness of Cu (nm)	Number of BP (M)	Resonant angle shift (deg.)	Sensitivity (deg./RIU)	FWHM (deg.)	DA (1/deg.)	QF (1/RIU)
35	1	6.45	83.03	4.4	0.227	18.87
40	1	6.61	85.09	3.97	0.251	21.43
45	1	6.70	86.25	3.27	0.305	26.37
50	1	6.74	86.76	2.76	0.362	31.43
35	3	6.83	87.92	6.44	0.155	13.65
40	3	6.99	89.98	4.92	0.203	18.28
45	3	7.09	91.27	3.83	0.261	23.83
50	3	7.17	92.30	3.25	0.307	28.4
35	6	7.4	95.26	7.76	0.128	12.27
40	6	7.73	99.51	6.17	0.162	16.12
45	6	8.01	103.11	4.4	0.227	23.43
50	6	8.12	104.53	4.35	0.229	24.02
35	9	8.35	107.49	9.31	0.107	11.54
40	9	8.81	113.41	7.95	0.125	14.26
45	9	9.31	119.85	6.45	0.155	18.58
50	9	9.63	123.97	6.28	0.159	19.74

different concentrations are plotted in Fig. 8. The red points represent the simulated data while the black curve represents the fitting equation. The fitting equation for the resonant angle-concentration relation is found as follows:

$$\theta_{res}(c) = 61.31 + 0.168\ c + 0.0011\ c^2 \tag{12}$$

where $\theta_{res}(c)$ is the resonant angle and C is the plasma concentration.

The agreement between the simulated data and the fitting equation is perfect. Resonant angle shift, sensitivity, FWHM, detection accuracy, and quality factor are calculated for the Au structure and presented in Table 6. It is observed that the sensitivity can be enhanced with the increase of the plasma concentration. The plasma concentration of 50 g/L corresponds to the highest sensitivity. The lowest concentrations correspond to the highest values of the detection accuracy and quality factor. In Fig. 9, the sensitivity, FWHM, detection accuracy, and quality factor are plotted versus the plasma concentration. In a similar manner to the sensitivity, the FWHM is enhanced with the increase of concentration.

Figure 10 shows the reflected intensity of the proposed SPR sensor for the Ag structure at different concentrations of plasma. The concentration dependence of the resonant angles is shown in Fig. 11. The red points represent the simulated data and the black curve represents the fitting equation. The fitting equation for the resonant angle-concentration relation is found as follows:

$$\theta_{res}(c) = 57.15 + 0.152\ c + 0.0004\ c^2 \tag{13}$$

Good agreement between the simulated data (red points) and the fitting equation (black curve) is observed in Fig. 11. Resonant angle shift, sensitivity, FWHM, detection accuracy, and quality factor are calculated for the Ag-structure and presented in Table 7. As can be observed, the sensitivity is improved with the growth of the concentration. A highest sensitivity of 93.07 deg./RIU corresponds to a plasma concentration of 50 g/L whereas the highest detection accuracy and quality factor correspond to the lowest concentration. The sensitivity, FWHM, detection accuracy, and quality factor are all shown in Fig. 12 versus the plasma concentration.

The reflected intensity of the Cu-structure for different concentrations of blood plasma is illustrated in Fig. 13 and the resonant angles corresponding to different concentrations are shown in Fig. 14. The red points represent the simulated data while the black curve represents the fitting equation. The fitting equation for the resonant angle-concentration relation is found as follows:

$$\theta_{res}(c) = 61.58 + 0.164\ c + 0.0012\ c^2 \tag{14}$$

The agreement between the simulated data and the fitting equation is perfect. Resonant angle shift, sensitivity, FWHM, detection accuracy, and quality factor are calculated for the Cu-structure and presented in Table 8. The sensitivity shows an essential enhancement with the increase of the plasma concentration. The plasma concentration of 50 g/L corresponds to the highest sensitivity of 123.97. The highest values of the detection accuracy and quality factor correspond to the lowest concentrations. In Fig. 15, the

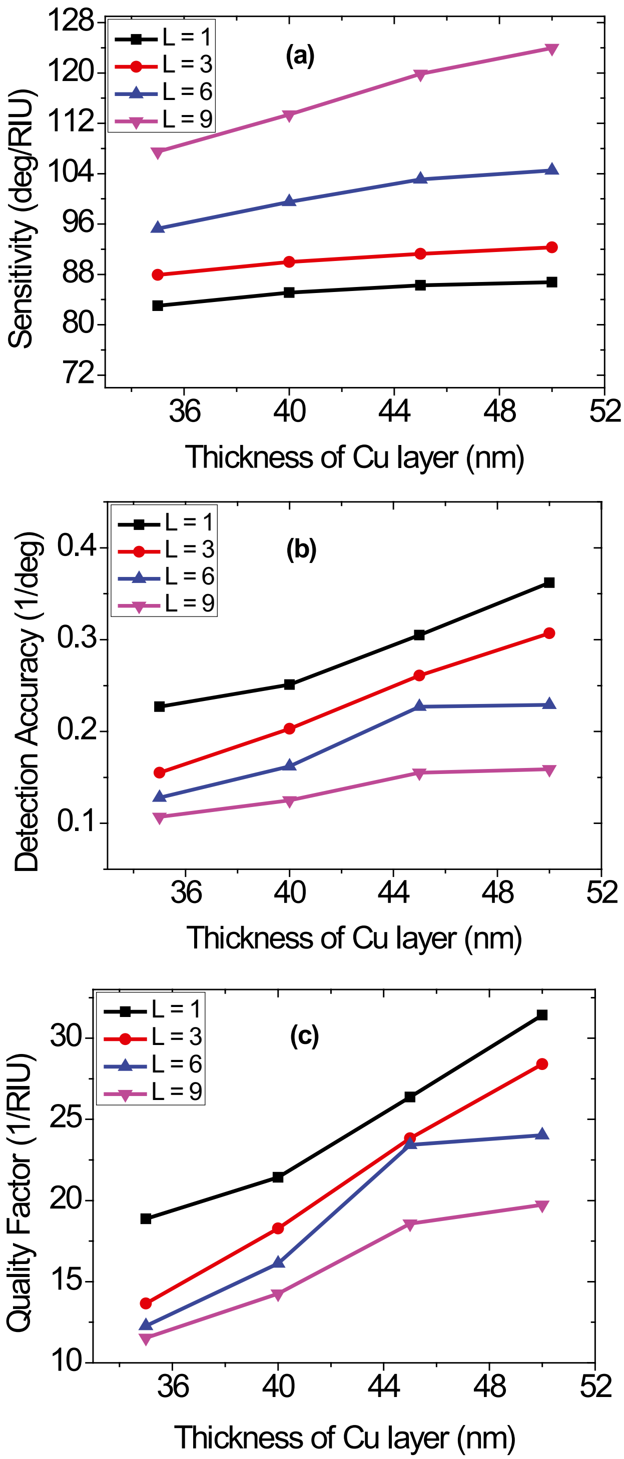

Fig. 6 The sensitivity (**a**), detection accuracy (**b**), and quality factor (**c**) versus the Cu layer thickness for different numbers of BP layers at a light wavelength of 632.8 nm

sensitivity, FWHM, detection accuracy, and quality factor are plotted versus the plasma concentration. In a similar manner to the sensitivity, the FWHM is enhanced with the increase of the plasma concentration.

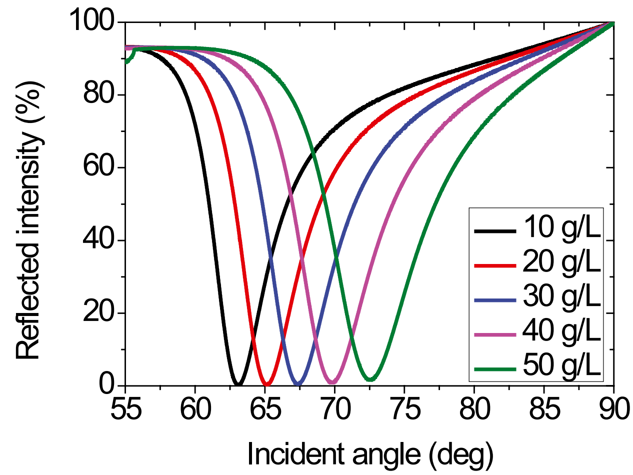

Fig. 7 Reflected intensity versus the angle of incidence for the proposed SPR sensor at different plasma concentrations at $\lambda = 632.8$ nm, $h_{Au} = 50$ nm, and $M = 9$

A comparison of the current work sensitivity with those of the most recent published SPR sensors is presented in Table 9. It shows the structure used in each work and the sensitivity obtained. It is clear that the sensitivity realized in the current work is the highest.

It is a good idea to provide the designer with some suggestions to make the proposed sensor easier to make. First, a thin layer of 50 nm of the metal has to be deposited on the N-FK51A glass prism. The deposition techniques that are usually used are vacuum thermal evaporation, electron beam evaporation, ion plating evaporation, laser beam evaporation, etc. The desired number of layers of black phosphor is then deposited on the top of the metal layer using chemical vapor deposition. A blood sample is then placed on top of

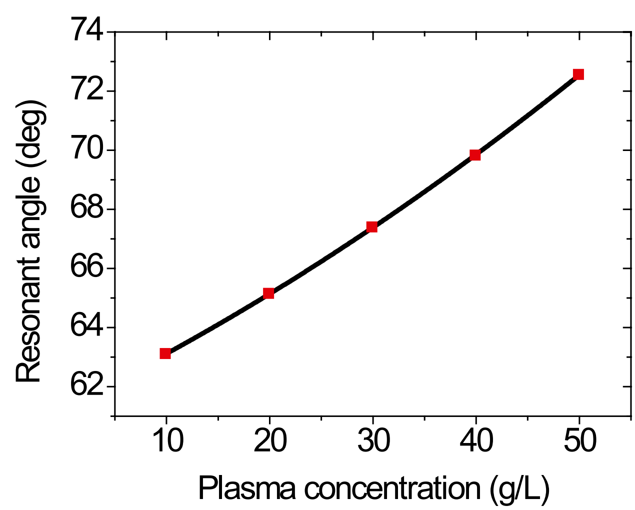

Fig. 8 Resonant angle versus the concentration of plasma for the proposed SPR sensor at $\lambda = 632.8$ nm, $h_{Au} = 50$ nm, and $M = 9$

Table 6 Some parameters to measure the performance of the proposed sensor at $\lambda = 632.8$ nm, $h_{Au} = 50$ nm, and $M = 9$ for different concentrations of plasma

Plasma concentration (g/L)	10	20	30	40	50
Refractive index	1.34401	1.36343	1.38285	1.40227	1.42169
Resonant angle (deg.)	63.11	65.15	67.4	69.83	72.56
Resonant angle shift (deg.)	-	2.04	4.29	6.72	9.45
Sensitivity (deg./RIU)	-	105.04	110.45	115.34	121.65
FWHM (deg.)	4.25	4.73	5.35	5.88	6.12
Detection accuracy	0.235	0.211	0.186	0.170	0.163
Quality factor	-	22.20	20.64	19.61	19.87

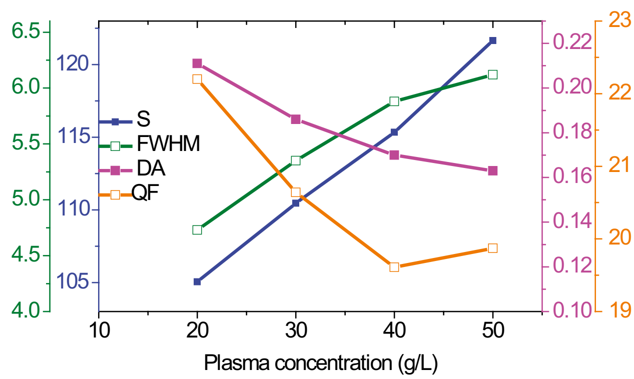

Fig. 9 Sensitivity, quality factor, FWHM, and detection accuracy versus the concentration of plasma for proposed SPR sensor at $\lambda = 632.8$ nm, $h_{Au} = 50$ nm, and $M = 9$

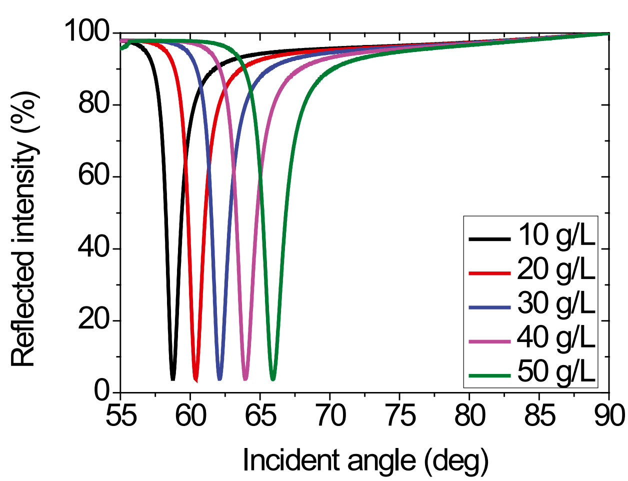

Fig. 10 Reflected intensity versus incident angle for the proposed SPR sensor with different concentrations at $\lambda = 632.8$ nm, $h_{Ag} = 50$ nm, and $M = 9$

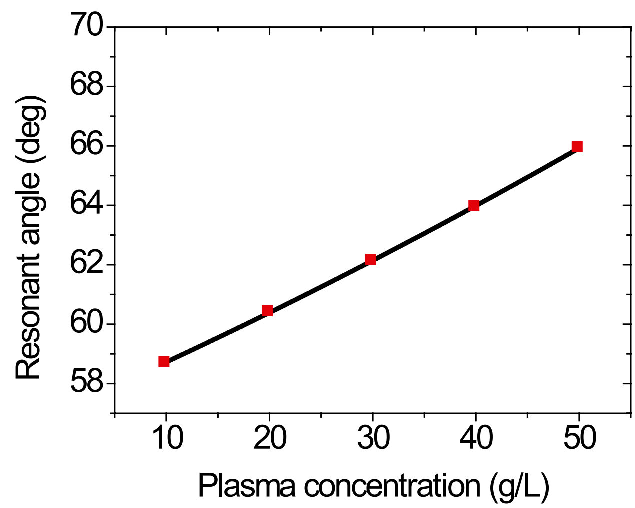

Fig. 11 Resonant angle versus the concentration of plasma for the proposed SPR sensor at $\lambda = 632.8$ nm, $h_{Ag} = 50$ nm, and $M = 9$

Table 7 Some parameters to measure the performance of the proposed sensor at $\lambda = 632.8$ nm, $h_{Ag} = 50$ nm, and M = 9 for different concentrations of plasma

Plasma concentration (g/L)	10	20	30	40	50
Refractive index	1.34401	1.36343	1.38285	1.40227	1.42169
Resonant angle (deg.)	58.71	60.42	62.14	63.96	65.94
Resonant angle shift (deg.)	-	1.71	3.43	5.25	7.23
Sensitivity (deg./RIU)	-	88.05	88.92	90.11	93.07
FWHM (deg.)	1.05	1.15	1.25	1.40	1.51
Detection accuracy	0.952	0.869	0.8	0.714	0.662
Quality factor	-	76.56	71.13	64.36	61.63

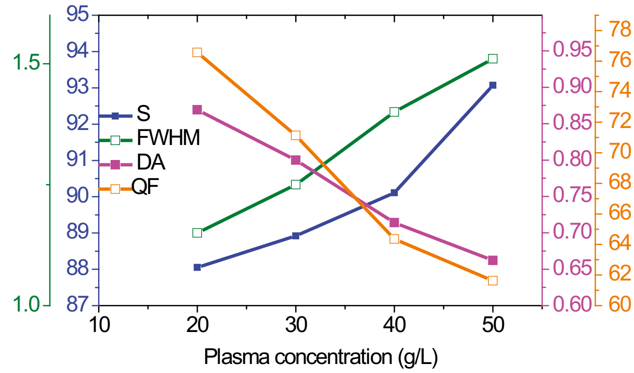

Fig. 12 Sensitivity, quality factor, FWHM, and detection accuracy versus the concentration of plasma for the proposed SPR sensor at $\lambda = 632.8$ nm, $h_{Ag} = 50$ nm, and M = 9

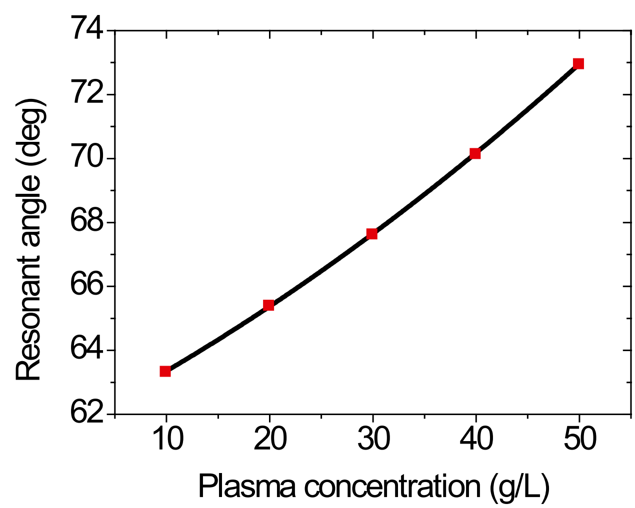

Fig. 14 Resonant angle versus the concentration of plasma for the proposed SPR sensor at $\lambda = 632.8$ nm, $h_{Cu} = 50$ nm, and M = 9

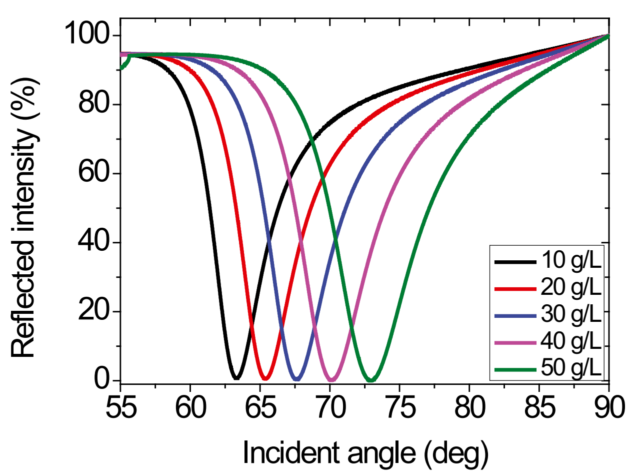

Fig. 13 Reflected intensity versus incident angle for the proposed SPR sensor with different concentrations at $\lambda = 632.8$ nm, $h_{Cu} = 50$ nm, and M = 9

the black phosphor material. Through the glass prism, the He–Ne laser is directed onto the metal film, and the subsequent reflection is monitored.

Table 8 The performance of the sensor with the variation of plasma concentration at λ = 632.8 nm, $h_{Cu}=50$ nm, and M = 9 for different concentrations of plasma

Plasma concentration (g/L)	10	20	30	40	50
Refractive index	1.34401	1.36343	1.38285	1.40227	1.42169
Resonant angle (deg.)	63.34	65.41	67.64	70.16	72.97
Resonant angle shift (deg.)	–	2.07	4.3	6.82	9.63
Sensitivity (deg./RIU)	–	106.59	110.71	117.06	123.97
FWHM (deg.)	4.21	4.6	5.06	5.53	6.28
Detection accuracy	0.237	0.217	0.197	0.180	0.159
Quality factor	–	23.17	21.87	21.16	19.74

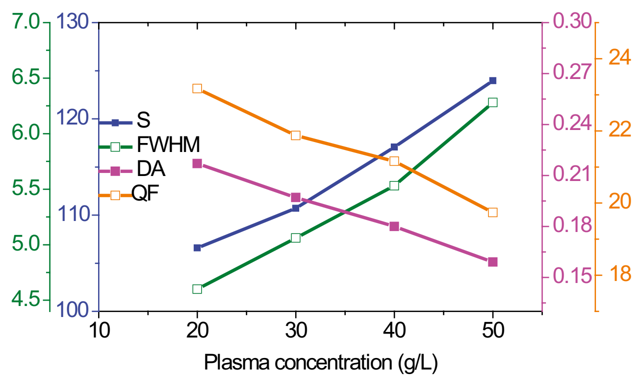

Fig. 15 Sensitivity, quality factor, FWHM, and detection accuracy versus the concentration of plasma for proposed SPR sensor at λ = 632.8 nm, $h_{Cu}=50$ nm, and M = 9

Conclusion

We have proposed an SPR-based biosensor for the detection of blood plasma. The structure of the proposed sensor is a low refractive index prism/metal/BP/sensing medium. Four metals, different numbers of BP layers, and different plasma concentrations have been tested to find out the structure with the highest performance. We found that structures with the BP layer have better performance than those without a BP layer. Cu-structure has shown the highest sensitivity of 123 deg./RIU while the Ag structure has shown the highest quality factor of 176.02 and detection accuracy of 2.325. The Ag structure has also shown the sharpest resonance dip with a FWHM of 0.43. The highest sensitivity was obtained at a Cu layer thickness of 50 nm and a number of BP layers

Table 9 Comparing the current work sensitivity with the most recent works

Structure of SPR	Year	Sensitivity (deg./RIU)	References
Au-MoS_2-graphene based hybrid SPR biosensor	2017	89.29	[33]
SPR sensor employing the structure ZnO–Au-MoS_2-graphene	2018	101.58	[34]
MoS_2-graphene hybrid-based fiber optic SPR biosensor	2017	105.71	[35]
SPR sensor employing graphene tri sheets	2019	121.67	[36]
SPR optical sensor using a thin layer of plasma	2021	103	[13]
SPR sensor employing black phosphor sheets	2022	124	Current work

of 9. The highest detection accuracy and quality factor were obtained at an Ag layer thickness of 50 nm and a monolayer of BP. As the concentration of the plasma increases, the sensitivity can be enhanced.

Author Contribution All authors contributed to the study conception and design. Mathematical derivation and part of the editing were performed by Abdulkarem H. M. Almawgani and Malek G. Daher. The code and part of the editing were performed by Sofyan A. Taya and Melad M. Olaimat. The first draft of the manuscript was written by Adam R. H. Alhawari and Ilhami Colak. Discussion of the results was performed by Sofyan A Taya. All authors commented on previous versions of the manuscript. All authors read and approved the final manuscript.

Funding The authors are thankful to the Deanship of Scientific Research at Najran University for funding this work under the Research Groups Funding program grant code (NU/RG/SERC/11/16).

Availability of Data and Material Detail about data has been provided in the article.

Code Availability The used code can be obtained from the corresponding author upon request.

Declarations

Competing interests The authors declare no competing interests.

Ethics Approval This study does not require ethics approval.

Consent to Participate No consent to participate is required for this study.

Consent for Publication No consent for publication is required for this study.

Conflict of Interest The authors declare no competing interests.

References

1. Liedberg B, Nylander C, Sundstrom I (2005) Surface plasmon resonance for gas detection andiosensing. Sens Actuators B Chem 4:299–304
2. Jorgenson RC, Yee SS (1993) A fiber-optic chemical sensor based on surface plasmon resonance. Sens Actuators B Chem 12:213–220
3. Yupapin P, Trabelsi Y, Vigneswaran D, Taya SA, Daher MG, Colak I (2022) Ultra-high-sensitive sensor based on surface plasmon resonance structure having Si and graphene layers for the detection of chikungunya virus. Plasmonics. https://doi.org/10.1007/s11468-022-01631-w
4. Srivastava T, Purkayastha A, Jha R (2016) Graphene based surface plasmon resonance gas sensor for terahertz. Opt Quant Electron 48:334
5. Kretschmann E, Reather H (1968) Radiative decay of non-radiative surface plasmons excited by light. Z Naturforsch 23:2135–2221
6. Maurya JB, Prajapati YK (2016) A comparative study of different metal and prism in the surface plasmon resonance biosensor having MoS2-graphene. Opt Quant Electron 48:280
7. Maharana PK, Bhardwaj S, Jha R (2013) Electric field enhancement in surface plasmon resonance bimettalic configuration based on chalcogenide prism. J Appl Phys 114:014304
8. Daher MG, Taya SA, Colak I, Patel S, Olaimat MM, Ramahi O (2022) Surface plasmon resonance biosensor based on graphene layer for the detection of waterborne bacteria. J Biophotonics 15:e202200001
9. Li L, Yu Y, Ye GL, Ge Q, Ou X, Wu H, Feng D, Chen XH, Zhang Y (2014) Black phosphorus field-effect transistors. Nat Nanotechnol 9:372–377
10. Qiao J, Kong X, Hu ZX, Yang F, Ji W (2014) High-mobility transport anisotropy and linear dichroism in few-layer black phosphorus. Nat Commun 5:4475
11. Rodin AS, Carvalho A, Castro Neto AH (2014) Strain-induced gap modification in black phosphorus. Phys Rev Lett 112:176801
12. Wang X, Jones AM, Seyler KL, Tran V, Jia Y, Zhao H, Wang H, Yang L, Xu X, Xia F (2014) Highly anisotropic and robust excitons in monolayer black phosphorus. Nat Nanotechnol 10:517–521
13. Taya SA, Al-Ashi NE, Ramahi OM, Colak I, Amiri IS (2021) Surface plasmon resonance-based optical sensor using a thin layer of plasma. J Opt Soc Am B 38:2362–2367
14. Mao N, Tang J, Xie L, Wu J, Han B, Lin J, Deng S, Ji W, Xu K, Liu K, Tong L, Zhang J (2016) Optical anisotropy of BP in the visible regime. J Am Chem Soc 138:300–305
15. Verma VK, Pal S, Rizal C, Prajapati YK (2022) Tunable and sensitive detection of cortisol using anisotropic phosphorene with a surface plasmon resonance technique: numerical investigation. Magnetochemistry 8:31
16. Verma A, Sharma AK, Prajapati YK (2021) Simulation and analysis of SPR-based biosensor with borophene and antimonene layers. Opt Mater 119:111355
17. Sadeghi Z, Hajiani T, Shirkani H (2022) Optical properties of anisotropic phosphorene-graphene nanotubes and their application as label-free SPR biosensors in IR. Mater Sci Eng B 278:115615
18. Singh MK, Pal S, Verma A, Mishra V, Prajapati YK (2021) Sensitivity enhancement using anisotropic black phosphorus and antimonene in bi-metal layer-based surface plasmon resonance biosensor. Superlattices Microstruct 156:106969
19. Cho SY, Prajapati Y, Singh V, Saini J, Tripathi R (2016) Superior chemical sensing performance of black phosphorus: comparison with MoS2 and graphene. Adv Mater 28:7020–7028
20. Pal S, Verma A, Prajapati YK, Saini JP (2017) Influence of black phosphorous on performance of surface plasmon resonance biosensor. Opt Quant Electron 49:403
21. Khandelwal A, Mani H, Karigerasi MH, Lahiri I (2017) Phosphorene–the two-dimensional black phosphorous: properties, synthesis and applications. Mater Sci Eng B 221:17–34
22. Yasaei P, Behranginia A, Foroozan T, Asadi M, Kim K, Araghi FK, Khojin AS (2015) Stable and selective humidity sensing using stacked black phosphorus flakes. ACS Nano 9:9898–9905
23. Singh Y, Raghuwanshi SK (2019) Sensitivity enhancement of the surface plasmon resonance gas sensor with black phosphorus. IEEE Sens Lett 3:1–4
24. Kumar V, Brent JR, Shorie M, Kaur H, Chadha G, Thomas AG et al (2016) Nanostructured aptamer-functionalized black phosphorus sensing platform for label-free detection of myoglobin, a cardiovascular disease biomarker. ACS Appl Mater Interfaces 8:22860–22868
25. Wood JD, Wells SA, Jariwala D, Chen K-S, Cho E, Sangwan VK et al (2014) Effective passivation of exfoliated black phosphorus transistors against ambient degradation. Nano Lett 14:6964–6970
26. Lee HU, Park SY, Lee SC, Choi S, Seo S, Kim H et al (2016) Black phosphorus (BP) nanodots for potential biomedical applications. Small 12:214–219

27. Srivastava T, Jha R (2018) Black phosphorus: a new platform for gaseous sensing based on Surface Plasmon Resonance. IEEE Photonics Technol Lett 30:319–322
28. Elias DC, Gorbachev RV, Mayorov AS, Morozov SV, Zhukov AA, Blake P, Ponomarenko LA, Grigorieva IV, Novoselov KS, Guinea F, Geim AK (2011) Dirac cones reshaped by interaction effects in suspended graphene. Nat Phys 7:701–704
29. Panda A, Pukhrambam PD, Keiser G (2020) Performance analysis of graphene-based surface plasmon resonance biosensor for blood glucose and gas detection. Appl Phys A 126:1–12
30. Pal S, Verma A, Saini JP, Prajapati YK (2019) Sensitivity enhancement using silicon black phosphorous–TMDC coated surface plasmon resonance biosensor. IET Optoelectron 13:196–201
31. Almawgani A, Taya SA, Daher MG, Colak I, Wu F, Patel SK (2022) Detection of glucose concentration using a surface plasmon resonance biosensor based on barium titanate layers and molybdenum disulphide sheets. Phys Scr 97:065501
32. Wu L, Chu HS, Koh WS, Li EP (2010) Highly sensitive graphene biosensors based on surface plasmon resonance. Opt Express 18:14395–14400
33. Rahman MS, Anower MS, Rahman MK, Hasan MR, Hossain MB, Haque MI (2017) Design and numerical analysis of highly sensitive Au-MoS2-graphene based hybrid surface plasmon resonance biosensor. Opt Commun 396:36–43
34. Kushwaha AS, Kumar A, Kumar R, Srivastava SK (2018) A study of surface plasmon resonance (SPR) based biosensor with improved sensitivity. Photonics Nanostruct Fundem Appl 31:99–106
35. Rahman MS, Anower MS, Rahman MK, Hasan MR, Hossain MB, Haque MI (2017) Modeling of a highly sensitive MoS2-Graphene hybrid based fiber optic SPR biosensor for sensing DNA hybridization. Optik 140:989–997
36. Hossain MB, Mehedi IM, Moznuzzaman M, Abdulrazak LF, Hossain MA (2019) High performance refractive index SPR sensor modeling employing graphene tri sheets. Results Phys 15:102719